Chinese Chemical Letters 37 (2026) 111905

Contents lists available at ScienceDirect

Chinese Chemical Letters

journal homepage: www.elsevier.com/locate/cclet

Interface challenges of solid-state electrolytes/lithium metal anode: From origin analysis, failure mechanism to interface optimization strategies

Dongfan Li[a], Jinlong Lv[a], Jian-Cang Wang[b], Jiaxiang Liu[a], Huizhe Niu[a], Lu Yang[a], Hao Luo[a], Du Lv[a], Lichun Niu[a], Zemin He[a,*], Zongcheng Miao[c,*]

[a] Shaanxi Key Laboratory of Liquid Crystal Polymer Intelligent Display, Key Laboratory of Liquid Crystal Polymers based Flexible Display Technology in National Petroleum and Chemical Industry, Technological Institute of Materials & Energy Science (TIMES), Xijing University, Xi'an 710123, China
[b] School of Materials Science and Engineering, Northeastern University, Shenyang 110819, China
[c] School of Artificial Intelligence, Optics and ElectroNics (iOPEN), Northwestern Polytechnical University, Xi'an 710072, China

ARTICLE INFO

Article history:
Received 29 June 2025
Revised 22 September 2025
Accepted 27 September 2025
Available online 29 September 2025

Keywords:
All-solid-state lithium metal batteries
Solid-state electrolytes
Lithium metal anode
Interfacial issues
Optimization strategies

ABSTRACT

The advent of all-solid-state lithium metal batteries (ASSLMBs) holds promise for overcoming the safety hazards and energy density limitations faced by traditional lithium-ion batteries, thereby advancing the industrialization of next-generation energy storage technologies with high safety and specific energy. However, during practical application, three core challenges persist at the interface between the solid-state electrolytes (SSEs) and the lithium metal anode (LMA): Poor physical contact, interfacial side reactions, and growth of lithium dendrites. These interfacial issues constrain the overall performance of ASSLMBs and impede the commercialization process of this battery system. This review begins by examining the underlying mechanisms responsible for the interfacial problems between SSEs and LMA. Building on this foundation, optimization strategies and recent research progress are systematically introduced, classified according to the interfacial components: SSE-side optimizations, interface engineering, and LMA-side treatments. Finally, future research directions, strategies, and optimization schemes addressing the interfacial challenges between SSEs and LMA are prospected. This analysis aims to facilitate critical breakthroughs in the stability, cycling lifespan, and energy density of ASSLMBs, promoting their transition from laboratory innovation to commercial application.

© 2025 Published by Elsevier B.V. on behalf of Chinese Chemical Society and Institute of Materia Medica, Chinese Academy of Medical Sciences.

1. Introduction

Electrochemical energy storage technology, as a critical enabler for energy structure transition, has demonstrated broad application prospects in recent years across domains such as smart grids, electric vehicles, and distributed energy systems [1]. Although conventional lithium-ion batteries dominate the market owing to their mature manufacturing processes and stable cycling performance, their inherent limitations—including safety hazards induced by flammable liquid electrolytes, theoretical energy density bottlenecks (typically ~200–300 Wh/kg for common systems), and performance degradation at low temperatures—render them increasingly inadequate to meet the heightened demands for energy storage technologies in the context of carbon neutrality [2,3]. ASSLMB technology addresses these challenges by employing SSE systems as lithium-ion transport media. This approach not only fundamentally eliminates the thermal runaway risks associated with traditional liquid electrolytes but also enables synergistic design with high-voltage cathode materials (*e.g.*, lithium-rich manganese-based and sulfide cathodes) and ultrathin LMAs (theoretical capacity: 3860 mAh/g) [4]. Consequently, it paves a new pathway toward achieving battery systems with energy densities exceeding 500 Wh/kg, thereby accelerating the industrialization process of next-generation energy storage technologies characterized by enhanced safety and high specific energy.

The technological innovation of ASSLMBs is reflected in two aspects: In battery structure, replacing liquid electrolytes and separators with SSEs systems reconstructs the internal battery architecture [5]. This transformation not only eliminates the flammability risk of organic solvents but also reduces the proportion of inactive materials in the battery system by 30%–40%, improves spatial utilization in the battery structure, and provides higher struc-

* Corresponding authors.
E-mail addresses: zeminhe315@126.com (Z. He), miaozongcheng@nwpu.edu.cn (Z. Miao).

https://doi.org/10.1016/j.cclet.2025.111905
1001-8417/© 2025 Published by Elsevier B.V. on behalf of Chinese Chemical Society and Institute of Materia Medica, Chinese Academy of Medical Sciences.

tural strength compared to traditional battery structures; In electrode material selection, the use of SSEs enables the introduction of high-energy-density electrode materials into battery systems, providing more options for designing high-energy-density battery systems [6,7].

SSEs, as the core component of ASSLMBs, can be primarily categorized into inorganic SSEs, organic SSEs, and organic-inorganic SSEs based on material types: (1) Inorganic SSEs, represented by sulfide-, oxide-, and halide-based SSEs (*e.g.*, garnet-type $Li_7La_3Zr_2O_{12}$, sulfide $Li_{10}GeP_2S_{12}$, and halide Li_3InCl_6), become the preferred choice for high-power batteries due to their high ionic conductivity (10^{-4}–10^{-2} S/cm) and excellent thermal stability (decomposition temperature > 500 °C) [8,9]. (2) Organic SSEs, mainly polymer-based systems such as poly(ethylene oxide) (PEO) and poly(vinylidene fluoride) (PVDF), achieve lithium-ion conduction through the movement of flexible chain segments [10]. The flexible molecular chains endow organic SSEs with inherent flexibility, giving them natural advantages in electrode wettability and film processability, making them shine brilliantly in the field of flexible batteries. (3) Organic-inorganic composite SSEs incorporate nano-ceramic fillers (*e.g.*, LLZO, $Li_{10}GeP_2S_{12}$) into polymer matrices, combining the high ionic conductivity of inorganic materials with the interfacial compatibility advantages of organic phases [11,12]. This "synergy of rigidity and flexibility" design strategy can effectively address challenges faced by single-type SSEs, enabling synergistic development of different SSE systems [13].

Despite numerous types of SSEs being developed for ASSLMBs, multiple issues have emerged during practical application. Although inorganic SSEs possess high ionic conductivity and thermal stability, their intrinsic defects hinder commercialization [14]. Sulfide and halide SSEs both exhibit water instability and are prone to hygroscopic oxidation in air. Furthermore, inorganic systems universally face processing challenges: Sulfide SSEs require inert atmosphere preparation, while oxide SSEs need high-temperature sintering, both conflicting with existing battery production processes. Organic SSEs, despite their flexibility, are significantly constrained by narrow electrochemical stability windows and low room-temperature ionic conductivity. For instance, PEO's electrochemical window is limited by the oxidation potential of ether groups (~4.0 V), making it incompatible with high-voltage cathode materials [15]. PVDF-based electrolytes release HF during long-term cycling, corroding electrode surfaces. Beyond issues inherent to SSEs themselves, common challenges persist in ASSLMB systems, interfacial physical contact problems, electrochemical stability issues, and interfacial lithium dendrites formation during cathode/anode matching remain critical technical bottlenecks that severely constrain the industrialization progress of SSEs [16].

Among the numerous challenges in ASSLMB systems, the interfacial issues between SSEs and LMA severely constrain the electrochemical performance of ASSLMBs and represent a critical research focus [17,18]. First, as the essential pathway for lithium-ion transport, the physical contact at the interface directly affects ion conduction pathways. Unlike liquid electrolyte wetting of LMA, solid-solid contact inherently suffers from poor adhesion, reducing effective ion transport channels and increasing polarization voltage. Second, when paired with highly reactive LMA, SSEs undergo side reactions during electrochemical processes, generating detrimental SEI phases at the interface. Accumulation of these harmful SEI components severely degrades electrochemical performance, elevates interfacial resistance, and causes interfacial instability [19]. Third, inhomogeneous lithium deposition at the interface induces lithium dendrites formation. Although SSEs exhibit higher mechanical strength to suppress dendrites, lithium dendrites can still nucleate at interfacial defects or local heterogeneities. As dendrites grow, stress concentration and interfacial damage occur, increasing internal resistance or causing direct short circuits. Dendrite penetration remains the core safety hazard threatening battery reliability and cycle life, representing the decisive factor limiting ASSLMBs' safety [20]. Therefore, understanding interfacial mechanisms through advanced characterization techniques (*e.g.*, *in situ* SEM, *in situ* XPS, and *in situ* EIS) and developing context-specific strategies to optimize SSEs/LMA interfaces represents an urgent requirement for current development.

The interfacial failure mechanisms between SSEs and LMA, as a core issue constraining ASSLMBs' performance, have garnered significant attention in recent years. However, compared to extensive research on cathode interfacial side reactions and their modulation strategies [21–23], studies focusing on anode interfacial properties remain notably underdeveloped. Not only that, some existing literatures focuse more on introducing the overall issues and modification strategies of ASSLMB, without conducting in-depth discussions and analyses on the interface failure mechanism and interface modification strategies between SSEs and LMA [24,25]. Furthermore, some publications are dated and fail to incorporate recent methodological advances and novel optimization strategies [26–28]. Addressing these gaps, this work: (1) Distinctively departs from conventional broad-scope reviews by conducting an in-depth, systematic analysis of SSEs/LMA interfacial failure mechanisms—from their origins to dynamic evolution processes. (2) Summarizes targeted optimization strategies based on clarified failure mechanisms, while innovatively proposing applications of interdisciplinary approaches, systematic material screening, and integrated interface design for resolving interfacial challenges. (3) Systematically evaluates the technical bottlenecks, applicability scopes, and implementation potential of existing optimization strategies, while providing forward-looking research and development recommendations for core interfacial issues. This article aims to establish a scientific foundation and offer fresh perspectives for resolving interfacial failure challenges and developing practically viable interface regulation technologies, thereby facilitating the industrialization of SSEs in high-safety, long-cycle-life ASSLMBs (Fig. 1) [29–38].

2. Interfacial challenges between SSEs and LMA

Interfacial issues between SSEs and LMA constitute the core challenge constraining ASSLMBs' performance. Among the numerous obstacles in pairing SSEs with LMA, poor physical contact, interfacial side reactions, and lithium dendrites formation emerge as the three primary challenges [39,40]. (1) Physical contact between SSEs and LMA serves as the prerequisite for electrochemical reactions. Poor solid-solid interfacial contact reduces lithium-ion transport pathways, leading to a sharp increase in interfacial resistance and diminished energy efficiency of the battery system. (2) Side reactions arising from thermodynamic instability at the SSEs/LMA interface severely disrupt electrochemical processes. Electronically insulating byproducts not only increase interfacial resistance but also consume active materials during their formation [41]. (3) Lithium dendrites formation at the interface critically compromises interfacial stability and overall battery integrity. Dendrite growth induces internal short circuits and thermal runaway. Moreover, formed dendrites gradually transform into "dead lithium," causing irreversible lithium loss within the battery system (Fig. 2).

2.1. Poor physical contact

In ASSLMB systems, lithium ions migrate between the cathode and anode through SSEs under an electric field. The physical contact points between SSEs and LMA directly serve as interfacial transport pathways for lithium ions, making solid-solid physical contact a prerequisite for electrochemical reactions [42]. Typically,

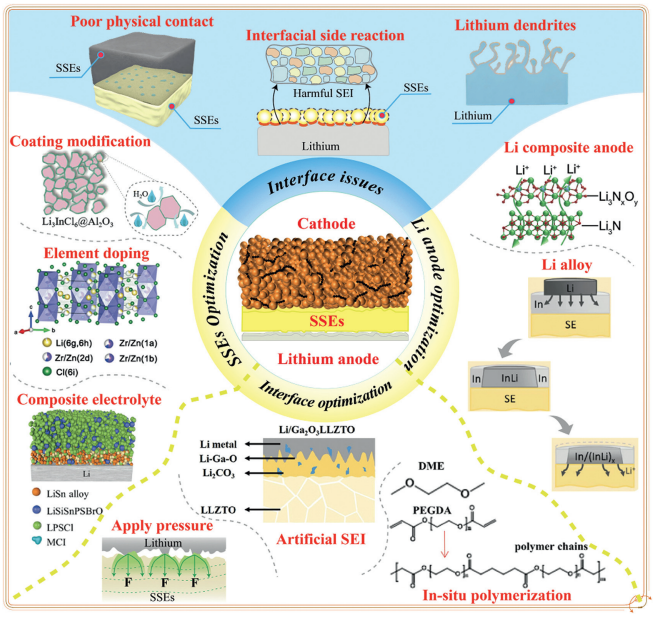


Fig. 1. Summary overview diagram of the core content of this article. Interfacial challenges and corresponding optimization strategies between SSEs and LMA. Reproduced with permission [29]. Copyright 2022, The American Association for the Advancement of Science. Reproduced with permission [30]. Copyright 2017, Springer Nature. Reproduced with permission [31]. Copyright 2021, Wiley-VCH. Reproduced with permission [32]. Copyright 2025, Wiley-VCH. Reproduced with permission [33]. Copyright 2025, Wiley-VCH. Reproduced with permission [34]. Copyright 2021, American Chemical Society. Reproduced with permission [35]. Copyright 2022, American Chemical Society. Reproduced with permission [36]. Copyright 2024, Wiley-VCH. Reproduced with permission [37]. Copyright 2024, Wiley-VCH. Reproduced with permission [38]. Copyright 2023, Royal Society of Chemistry.

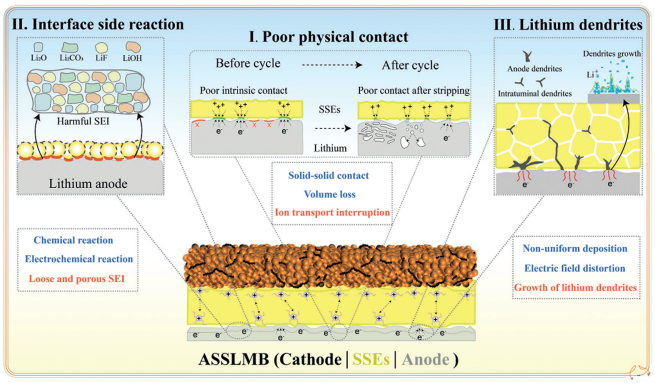


Fig. 2. Schematic illustration of interfacial challenges between SSEs and LMA.

both inorganic SSEs and solvent-free solid polymer electrolytes suffer from poor physical contact [43]. Even sulfide SSEs, which possess a softer consistency compared to oxide ceramic SSEs, cannot fully eliminate interfacial gaps with LMA. Consequently, it is imperative to elucidate the mechanisms underlying poor physical contact between SSEs and LMA from their origins.

To comprehensively clarify the interfacial physical contact issues between SSEs and LMA, the underlying mechanisms must be analyzed from multiple perspectives. Poor interfacial physical contact already exists before electrochemical reactions commence in ASSLMBs. First, intrinsic material property mismatches cause poor interfacial contact. As illustrated in Fig. 3a, interfaces between inorganic SSEs/solvent-free solid polymer electrolytes and LMA represent a typical solid-solid contact. Their contact effectiveness is far inferior to the solid-liquid infiltration contact achieved by traditional liquid electrolytes (Fig. 3b) [44]. Second, limitations in material processing techniques contribute to poor interfacial contact. Constraints in SSEs fabrication are primary factors: stress-induced grain boundary defects and pores during sintering of oxide SSEs, and voids from microbubbles in solution-cast polymer electrolytes, both degrade physical interfacial contact. Apart from the physical contact issues caused by SSEs, the surface of the LMA is not absolutely smooth, clean and defect-free either. LMA is soft in texture (with a Mohs hardness of only 0.6) and highly malleable. During the production process (such as rolling, cutting, and transfer), even slight mechanical stress (such as uneven rolling, fixture friction, and particles on the equipment surface) can cause surface damage. All these can lead to the interface not adhering closely (Fig. 3c), forming many tiny voids [29]. This reduces the ion transport channels, resulting in an increase in interface impedance. Moreover, during the subsequent cycling process, tiny voids can cause non-uniform deposition of lithium ions, serving as the formation and growth sites for lithium dendrites, leading to instability at the interface and throughout the entire battery system. The problem of poor interfacial physical contact arises from synergistic multi-faceted factors, severely constraining the applications.

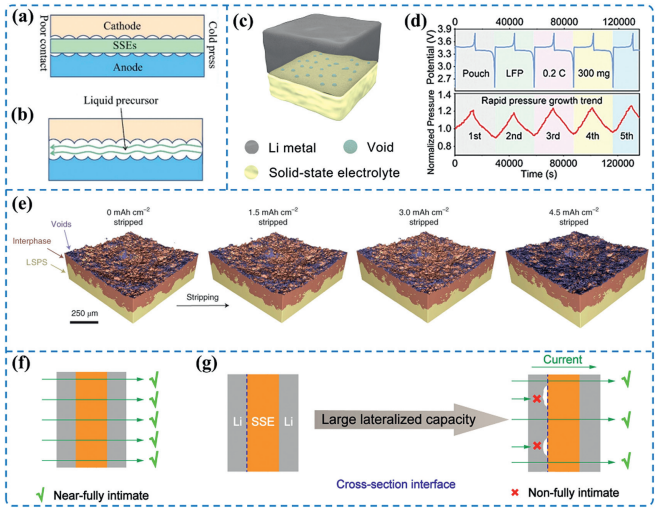


Fig. 3. (a) Schematic of solid-solid contact at the SSEs/LMA interface. (b) Schematic of solid-liquid infiltration contact between traditional liquid electrolyte and LMA. Reproduced with permission [44]. Copyright 2025, Elsevier. (c) Schematic illustrating interfacial gaps at the SSEs/LMA interface. Reproduced with permission [29]. Copyright 2022, The American Association for the Advancement of Science. (d) Stress evolution curves within LMA pouch cells *versus* cycle number. Reproduced with permission [46]. Copyright 2024, Wiley-VCH. (e) 3D-reconstructed view of the $Li_{10}SnP_2S_{12}$ interface after cycling at 1 mA/cm^2. Reproduced with permission [47]. Copyright 2021, Springer Nature. (f) Schematic of interfacial current density distribution under intimate contact conditions. (g) Schematic showing non-uniform current density distribution due to reduced contact points after cycling. Reproduced with permission [48]. Copyright 2023, Elsevier.

Beyond interfacial physical contact issues caused by intrinsic defects and manufacturing processes, volume changes in anode materials during electrochemical cycling also degrade physical contact with SSEs. In traditional liquid lithium-ion batteries, the liquid electrolyte can flow freely and fill the voids caused by volume changes in real time. In ASSLMBs, the rigid interface of solid-solid contact cannot adapt to the voids caused by the volume shrinkage of LMA, making the interface contact prone to local failure. Therefore, the ASSLMB system has a lower tolerance for volume changes. During the subsequent deposition of lithium ions, the presence of voids will lead to the non-uniform deposition of lithium ions, thereby causing the formation and growth of lithium dendrites. Whether it is the deposition process or the stripping process of lithium ions, volume changes will have an impact on the stability of the interface. He *et al.* [45] demonstrated that lithium deposi-

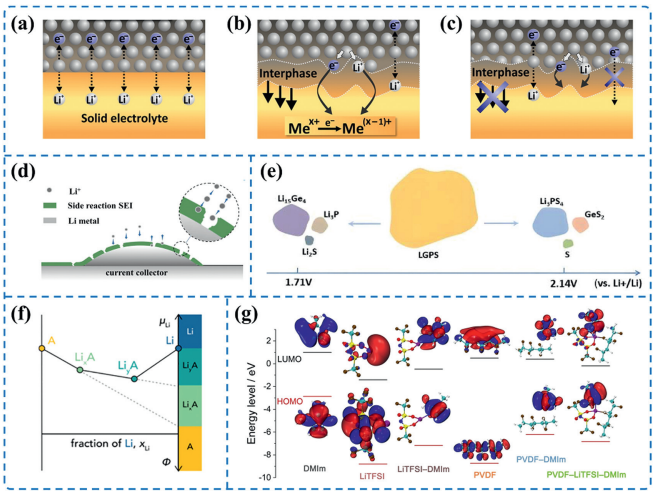


Fig. 4. (a) Schematic of an ideal stable interphase layer between SSEs and LMA. (b) Schematic of a semi-stable interphase layer formation. (c) Schematic of a destabilized interphase layer formation. Reproduced with permission [49]. Copyright 2015, Elsevier. (d) Schematic of unstable SEI formed by side reactions at the SSEs/LMA interface. Reproduced with permission [50]. Copyright 2024, Elsevier. (e) Schematic illustrating detrimental phase generation from side reactions in sulfide SSEs. Reproduced with permission [51]. Copyright 2023, Elsevier. (f) GPPD for lithium. Reproduced with permission [56]. Copyright 2025, American Chemical Society. (g) Electrochemical stability windows of components in solid polymer electrolyte systems. Reproduced with permission [58]. Copyright 2022, Wiley-VCH.

tion is irregular without deposition hosts. After 100 cycles in Li||Cu cells, newly deposited lithium layers can reach 100 μm thickness. To further investigate internal stress evolution, Chang *et al.* [46] examined stress changes in LMA pouch cells. As shown in Fig. 3d, this study visually confirms volume changes in LMA during cycling, where both stress buildup from expansion and contact loss from contraction detrimentally impact battery performance. During electrochemical processes, beyond anode volume changes, SSEs also undergo interfacial degradation, reducing physical contact and increasing local current density. Lewis *et al.* [47] applied X-ray tomography to sulfide-based ASSLMBs. The 3D-reconstructed interfacial microstructure after cycling at 1 mA/cm^2 (Fig. 3e) reveals significant voids/pores in sulfide SSEs post-deposition/dissolution, severely degrading interfacial contact. As cycling proceeds, interfacial contact further deteriorates. Compared to the original interfacial current density (Fig. 3f), reduced contact areas increase local current density at contact points (Fig. 3g), destabilizing the interface [48]. Therefore, developing effective strategies to mitigate mechanical failures from poor physical contact and maintain stable anode/SSEs interfacial integrity during cycling represents a pressing core challenge for high-performance, long-life ASSLMBs.

2.2. Interfacial side reactions

In addition to poor physical contact, interfacial side reactions between SSEs and LMA constitute a key obstacle to the practical application of ASSLMBs. Interfacial side reactions cause severe interfacial damage, significantly reducing the electrochemical performance of battery systems. Wenzel *et al.* [49] divided the interface between SSEs and LMA into three categories. Fig. 4a shows a stable interface state, corresponding to an ideal state where only lithium-ion transport occurs without charge exchange at the interface between SSEs and LMA. Fig. 4b shows a semi-stable interface state where partial charge transfer occurs at the interface. Fig. 4c shows a completely destabilized state where severe side reactions occur at the interface, leading to extreme degradation of interfacial performance, which seriously affects the electrochemical performance of ASSLMB systems. In current research, scientists categorize the mechanisms of interfacial side reactions into two types: chemical reactions and electrochemical side reactions. Chemical reactions refer to direct redox reactions caused by a chemical potential mismatch between SSEs and LMA. Electrochemical side reactions refer to parasitic reactions driven by electrochemical potential during operation. As shown in Fig. 4d, both types of interfacial side reactions generate detrimental phases that accumulate at the interface, forming a loose and porous SSEs interface (SEI), resulting in deteriorated stability at the SSEs/LMA interface [50].

The occurrence of interfacial chemical reactions does not require applied voltage; the driving force is pure chemical potential. Although the reaction process is generally slow, it still causes interfacial damage. The essence of interfacial chemical reactions lies in the thermodynamic instability between lithium metal and SSEs. Highly reactive lithium metal (electrode potential: −3.04 V *vs.* SHE) undergoes direct redox reactions driven by Gibbs free energy when paired with SSEs. Different types of SSEs contain distinct redox-active groups or ions. (1) Sulfide SSEs: S^{2-} ions are easily reduced by lithium metal, generating byproducts such as Li_2S and Li_3P (Fig. 4e). Prolonged accumulation forms a loose, porous SEI. The byproduct Li_2S further induces additional chemical reactions producing H_2S, which corrodes the interface [50,51]. (2) Garnet-type oxide SSEs (*e.g.*, LLZO): Exhibit high stability against lithium. Minor chemical reactions between them are negligible. Trace Li_2CO_3 impurities on their surfaces further reduce side reactions with LMA. In oxide systems, element doping (*e.g.*, Ta) enhances lithium stability [52,53]. (3) Solid polymer electrolytes: Taking the current research hotspot PEO as an example, the highly reactive LMA will undergo side reactions with the ether oxygen groups (C–O-C) in PEO upon contact, generating by-products such as Li_2O, C_2H_4, and H_2 [54]. Li_2O is unstable, loose and porous, and has a low ionic conductivity. It adheres to the surface of the lithium anode, forming a poor SEI layer that hinders ion transport, increases interface resistance, and intensifies electrode polarization. The gaseous by-products such as C_2H_4 and H_2 generated will increase the internal pressure of the battery, posing a risk of thermal runaway, combustion, and even explosion, causing dual damage to the electrochemical performance and safety of the battery system. (4) Halide SSEs: Taking Li_3YCl_6 as an example, it will be slowly reduced to Y by the LMA, accompanied by the generation of a small amount of the product LiCl with a high ion migration barrier, which causes obstacles to lithium ion transport at the interface.

Beyond chemically driven interfacial reactions, electrochemical side reactions also occur between lithium metal and SSEs under electrochemical potential. The essence of interfacial electrochemical side reactions involves unintended redox reactions of lithium metal or electrolyte components induced by charge transfer during external electric field application. These reactions exhibit significant current density dependence. Notably, interfacial electrochemical side reactions inevitably coexist with chemical side reactions. Current research typically treats electrode materials as inert by neglecting slow chemical processes to isolate electrochemical mechanisms. Electrochemical stability windows are commonly employed to evaluate SSEs stability, necessitating systematic studies of their lowest unoccupied molecular orbital (LUMO) and highest occupied molecular orbital (HOMO) levels [55]. As shown in the grand potential phase diagram (GPPD) for lithium (Fig. 4f), when lithium deposition/stripping overpotential exceeds the electrochemical stability window, SSEs undergo redox reactions with lithium metal, generating detrimental phases that accumulate at the interface and impede normal lithium deintercalation/transport [56].

Wang *et al.* [57] systematically investigated electrochemical stability windows of inorganic SSEs, establishing a database covering over 1500 inorganic compounds. Pei *et al.* [58] summarized stability windows of key components in representative solid polymer electrolytes (Fig. 4g). In polymer systems, the overall electrochemi-

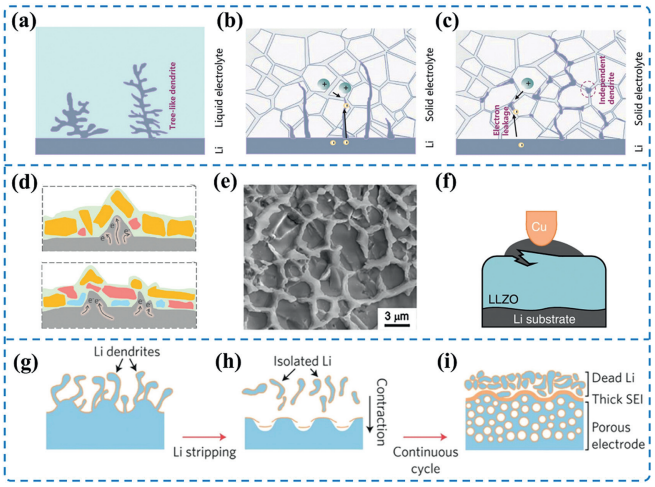


Fig. 5. (a) Schematic of an ideal stable interface between SSEs and LMA. (b) Schematic of semi-stable interface formation. (c) Schematic of destabilized interface formation. Reproduced with permission [59]. Copyright 2023, Wiley-VCH. (d) Schematic illustrating increased local current density due to dendrite-induced electric field distortion. Reproduced with permission [61]. Copyright 2025, Wiley-VCH. (e) SEM image of lithium dendrites growing along LLZO grain boundaries. Reproduced with permission [62]. Copyright 2025, American Chemical Society. (f) Schematic showing microcrack propagation in LLZO caused by lithium deposition. Reproduced with permission [63]. Copyright 2022, Springer Nature. (g) Schematic of lithium dendrites morphology. (h) Schematic of "dead lithium" formation during stripping. (i) Schematic of "dead lithium layer" accumulation after multiple deposition/stripping cycles. Reproduced with permission [30]. Copyright 2017, Springer Nature.

cal stability window is determined by its least stable component—a principle equally applicable to composite SSEs. These studies provide critical insights for resolving electrochemical stability challenges at lithium metal/SSEs interfaces.

2.3. Lithium dendrites

During electrochemical processes in ASSLMBs, the formation and growth of lithium dendrites pose a significant threat to interfacial stability between SSEs and LMA. Unlike lithium dendrites in conventional liquid batteries (Fig. 5a), dendrites in ASSLMBs preferentially grow unidirectionally (Fig. 5b) [59]. As dendrites propagate, they penetrate the dense structure of SSEs, compromising their integrity. This leads to internal short circuits and triggers thermal runaway, critically jeopardizing the safety of ASSLMBs. Therefore, elucidating lithium dendrites mechanisms from nucleation to growth at SSEs/LMA interfaces is of paramount importance.

Masias *et al.* determined the shear modulus of lithium to be 2.83 GPa using acoustic techniques [60]. Although the shear modulus of lithium dendrites has not been precisely measured, there are pores, grain boundaries and dislocation defects inside the dendrites, with a loose structure and poor continuity, which leads to its actual shear modulus being lower than that of bulk lithium metal. The shear modulus of inorganic SSEs is generally greater than 6 GPa, and that of oxide SSEs is even greater than 10 GPa, both more than twice the shear modulus of lithium dendrites. Theoretically, this can effectively inhibit the formation and growth of lithium dendrites. However, this theory studies the pure mechanical penetration of lithium dendrites under ideal conditions. In practical situations, the presence of lithium dendrites can still be observed at the interface between inorganic SSEs and the LMA. This is because microscopic defects at the interface between SSEs and the LMA, such as microcracks and tiny pores, can cause abnormally high local current density, leading to the priority occurrence of lithium deposition at the defect sites to form initial dendrites. After the initial dendrite formation, only a very small stress is needed to promote the lateral propagation of the crack, causing the crack to expand and thus leading to the further growth of lithium dendrites. This also explains why lithium dendrites are inevitable in inorganic SSEs.

There are two mechanisms for lithium dendrites generation in ASSLMBs: LMA-induced dendrites, as shown in Fig. 5b, and dendrites formed at grain boundaries and microcracks in inorganic SSEs (Fig. 5c). Detailed analysis follows. First, regarding the formation mechanism of LMA-induced dendrites: surface inhomogeneities, poor interfacial contact, and impurity phases formed by side reactions on LMA all cause non-uniform current distribution. This induces heterogeneous lithium deposition, forming initial dendrites. After initial dendrite formation, they disrupt the electric field distribution at the interface, causing local field distortion (Fig. 5d). This further exacerbates uneven lithium deposition, promoting dendrite growth while creating more nucleation sites, establishing a vicious cycle that severely degrades the interface [61].

Another type of lithium dendrites is formed at the grain boundaries of inorganic SSEs. Taking the typical LLZO as an example, by measuring the potential distribution at the grain boundaries with high-resolution kelvin probe force microscopy (KPFM), it can be found that the location of the electron leakage hotspots highly coincides with the formation location of lithium dendrites. This indicates that the high electronic conduction characteristics at the grain boundaries of LLZO play a significant role in the formation of lithium dendrites at the grain boundaries. The schematic diagram of lithium dendrites at grain boundaries is shown in Fig. 5e, which can cause severe damage to the interface between SSEs and the LMA [62]. Apart from the grain boundaries, the non-uniformly distributed electric fields existing at the inevitable micro-cracks and voids and other defects in SSEs can also induce non-uniform deposition of lithium ions, resulting in lithium dendrite problems. Gao *et al.* [63] visualized the lithium dendrites at the interface between SSEs and LMA through *in-situ* TEM. The research indicates that during high-speed deposition of lithium ions, the deposition of lithium dendrites accumulates local stresses ranging from GPa to 10 GPa at the micro-cracks of LLZO particles, causing lateral and longitudinal expansion of the microcracks. This ultimately led to the cracking of LLZO particles (Fig. 5f).

Beyond severely compromising interfacial stability, lithium dendrites at SSEs/LMA interfaces also cause active material loss. On one hand, dendrites formed within SSEs become electrochemically inactive, they no longer participate in lithium stripping and only receive deposited ions, evolving into continuously growing "dead lithium." On the other hand, dendrites generated on LMA may undergo brittle fracture during growth (Figs. 5g and h), forming isolated "dead lithium." This dead lithium can accumulate at interfaces, creating a "dead lithium layer" (Fig. 5i) that obstructs ion transport pathways, increases interfacial impedance, and reduces reversible capacity and cycle stability. Consequently, battery performance degrades rapidly, critically hindering the practical application and commercialization of ASSLMBs [30]. Therefore, optimizing the SSEs/LMA interface through multi-dimensional strategies, including anode optimization, electrolyte enhancement, and interfacial engineering, is paramount for enabling the transition of ASSLMBs from usable to reliable.

3. Optimization strategies

After clarifying the mechanisms underlying interfacial issues between SSEs and LMA, implementing targeted optimization strategies addressing these origins represents an effective approach to enhance ASSLMB electrochemical performance [64]. The core objective of interfacial optimization lies in achieving synergistic

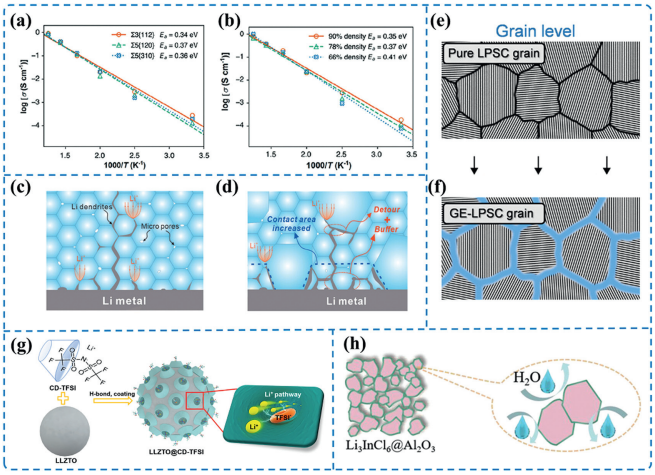


Fig. 6. (a) Ionic conductivity of lithium ions at the grain boundaries of Li_3InCl_6. (b) Ionic conductivity of lithium ions within the grain boundaries of Li_3InCl_6. Reproduced with permission [66]. Copyright 2023, Wiley-VCH. (c) Direct penetration of lithium dendrites through homogeneous LLZO grains. (d) Confined growth of lithium dendrites in LLZO with mixed large/small grains. Reproduced with permission [68]. Copyright 2024, Wiley-VCH. (e) Pristine Li_6PS_5Cl grains. (f) Core-shell coating layer on Li_6PS_5Cl grain surfaces. Reproduced with permission [71]. Copyright 2025, Wiley-VCH. (g) Coating optimization of $Li_{6.75}La_3Zr_{1.75}Ta_{0.25}O_{12}$ using functional supramolecules. Reproduced with permission [73]. Copyright 2023, Wiley-VCH. (h) Al_2O_3 coating on Li_3InCl_6 particles. Reproduced with permission [31]. Copyright 2021, Wiley-VCH.

development of mechanical compatibility and electrochemical stability through multidimensional optimization strategies, while simultaneously suppressing lithium dendrites formation/growth during operation [65].

Surveying current strategies, this review categorizes them into three types based on optimization targets: (1) SSEs-side optimizations: Optimizing electrolyte composition and structure *via* doping or compositing to enhance mechanical properties and chemical stability. (2) Interface-specific optimizations: Introducing functional interlayers or implementing *in situ* interfacial polymerization between SSEs and anodes. These approaches ensure efficient ion transport while providing physical isolation, improving interfacial contact, and inhibiting dendrites. (3) LMA-side optimizations: Employing lithium alloys or constructing 3D porous current collectors to regulate deposition behavior and reduce electrochemical reactivity, thereby minimizing side reactions and dendrite formation. These multiscale, multiphysics-coupled strategies will provide theoretical guidance and technical support for constructing highly stable, low-impedance solid-solid interfaces, ultimately advancing solid-state lithium batteries toward practical high-energy-density, long-cycle-life applications.

3.1. SSEs optimization strategies

3.1.1. Grain optimization

Optimizing grains and grain boundaries during SSEs production effectively enhances interfacial stability. Appropriately reducing particle size while maintaining ionic conductivity increases contact area with lithium metal, improving physical contact to reduce interfacial resistance and electrochemical polarization. Concurrently, finer particles enhance densification, reducing internal pores/defects and boosting mechanical strength to reinforce dendrite-blocking capability—thereby optimizing interfacial contact and improving ASSLMBs' performance/safety. Li *et al.* [66] demonstrated that in Li_3InCl_6, grain boundary ionic conductivity (Fig. 6a) and bulk ionic conductivity (Fig. 6b) are nearly identical, indicating that grain boundaries do not impede ion transport. Thus, grain refinement minimizes pores/defects blocking ion transport while optimizing interfacial contact. Xu *et al.* [67] investigated LLZO grain size effects: Smaller grains improve stress distribution but promote crack propagation, necessitating balanced optimization. Jia *et al.* [68] designed a hybrid microstructure with large/small grains in LLZO. Unlike single-grain structures where dendrites penetrate straight through (Fig. 6c), the mixed-grain boundaries (Fig. 6d) deflect dendrite growth, reducing penetration risk. Singh *et al.* [69] confirmed in Li_6PS_5Cl sulfide SSEs that grain refinement reduces bulk defects and enhances mechanical robustness.

Notably, grain refinement requires balancing size effects and processing stability. Excessive particle size reduction may induce agglomeration issues or exacerbate interfacial side reactions. Therefore, future research should prioritize appropriate process exploration, identifying optimal grain sizes or adopting hybrid grain combinations to synergistically optimize particle dimensions and interfacial characteristics, thereby advancing the practical implementation of ASSLMBs.

3.1.2. Coating optimization

Surface coating technology applied to SSEs offers a novel approach to optimize interfacial issues with LMA. The coating layer effectively isolates direct contact between lithium metal and SSEs, preventing electrochemical side reactions [70]. Simultaneously, for less stable SSEs like sulfides and halides, coating optimization enhances their stability toward water and oxygen, improving inherent robustness. In recent years, strategies optimizing interfacial properties through electrolyte coatings have gained significant attention. This technology shows promise for enhancing battery performance, extending cycle life, and improving safety.

Core-shell coating technology fundamentally hinges on the selection of coating materials. When selecting a coating material, it is essential to ensure that it does not adversely affect the lithium-ion conductivity of the SSEs. Secondly, a comprehensive consideration of its electrochemical stability, mechanical properties, and compatibility with the substrate material is required. Furthermore, coating strategies differ significantly depending on the type of SSEs. Coating optimization strategies are more commonly applied within inorganic SSE systems. For instance, as illustrated in Figs. 6e and f, Su *et al.* [71] constructed a Sn-Cl-S compound coating layer on the surface of Li_6PS_5Cl through a simple anion exchange reaction with Cl^- in $SnCl_4$. This coating exhibited a core-shell structure, enhancing the stability of the sulfide SSEs and effectively preventing lithium dendrites penetration. Similarly, within the sulfide SSEs system, Liu *et al.* [72] employed long-chain alkyl thiol (1-undecanethiol) coating, which significantly improved the chemical stability of the sulfide electrolyte when exposed to high-humidity environments. Lu *et al.* [73] utilized a functional supramolecular system composed of β-cyclodextrin (CD) and LiTFSI to coat $Li_{6.75}La_3Zr_{1.75}Ta_{0.25}O_{12}$, employing the coating scheme depicted in Fig. 6g. Remarkably, the coating layer not only did not impede lithium-ion transport but also exhibited higher ionic conductivity than the bulk material. Moreover, the presence of the coating expanded the electrochemical stability window of $Li_{6.75}La_3Zr_{1.75}Ta_{0.25}O_{12}$, thereby enhancing its overall electrochemical stability. For halide SSEs, which offer the advantages of simple synthesis and high ionic conductivity, their high reactivity with air and water severely hinders development. Wang *et al.* [31] addressed this by coating Li_3InCl_6 with Al_2O_3 to mitigate its side reactions with water (Fig. 6h). This approach provides a viable strategy for designing stable halide SSEs and developing suitable protective measures.

Current coating technologies still grapple with challenges related to coating thickness, processing techniques, and coating layer stability. Future research must transcend the limitations of "single-function optimization" and develop coating materials that integrate

high ionic conduction, robust mechanical compatibility, and high stability (*e.g.*, temperature-responsive shape-memory alloy coatings). This will enable the synergistic optimization of SSEs' coating technology and interfacial stability, facilitating a pivotal transition for surface coating technology from laboratory innovation to engineering applications.

3.1.3. Elemental doping optimization

Elemental doping for the intrinsic optimization of SSEs represents a core strategy for regulating interfacial physicochemical behaviors at the lattice scale. Its fundamental principle lies in optimizing the ionic conduction pathways, chemical activity, and mechanical strength of SSEs through approaches such as heterovalent ion substitution and vacancy engineering. This effectively mitigates challenges associated with solid-solid interfacial contact failure and side reactions [74]. Elemental doping optimization strategies are typically applied within inorganic SSE systems. Specifically, this approach encompasses diverse methodologies: doping can be designed to target the enhancement of a specific property of the SSEs, or, through the judicious selection of dopant elements, it can concurrently improve multiple performance aspects (*e.g.*, achieving the synergistic enhancement of both ionic conductivity and electrochemical stability). Based on the type of dopant elements used, elemental doping optimization can be further categorized into single-element doping and multi-element co-doping.

For inorganic SSEs, elemental doping strategies can be employed to optimize the electrolyte itself, thereby enhancing its interfacial stability. Taking sulfide SSEs as an example, researchers frequently utilize elemental doping to improve their intrinsic stability against water. Zhou *et al.* [75] systematically investigated the electrolyte systems $Li_{7.3}P_{2.9}S_{10.75}X_{0.3}$ (X = F, Cl, Br, I) prepared *via* halogen element doping. Compared to the electrochemical stability window of LPSCl determined by Wu *et al.* (oxidation limit < 2.5 V *vs.* Li/Li^+) [76], the CV test results shown in Fig. 7a demonstrate that the $Li_{7.3}P_{2.9}S_{10.75}X_{0.3}$ systems achieve an electrochemical stability window up to 5 V, exhibiting excellent chemical stability. Zhang *et al.* [77] employed a co-doping strategy involving Sn^{2+} and F^-, as illustrated in Fig. 7b, to modify $Li_{10}GeP_2S_{12}$. The dopant elements substitute for partial Ge^{4+} and S^{2-} sites in $Li_{10}GeP_2S_{12}$, significantly reducing both the H_2O adsorption energy and the interfacial lithium vacancy formation energy. This optimization markedly enhances the stability of $Li_{10}GeP_2S_{12}$ towards humid air and lithium metal. Anderson *et al.* [78] comprehensively screened the effects of 59 dopants on LLZO, one of the most extensively studied oxide SSEs. This study provides a valuable database for dopant selection, offering insights into synergistically enhancing the ionic conductivity, intrinsic stability, and compatibility with LMA in SSEs through elemental doping.

Within halide SSE systems, elemental doping is also a common approach to enhance both ionic conductivity and electrochemical stability. Lei *et al.* [32] introduced Zn^{2+} doping into Li_2ZrCl_6, synthesizing $Li_{2.4}Zr_{0.8}Zn_{0.2}Cl_6$, whose crystal structure is depicted in Fig. 7c. The Zn^{2+} doping optimizes the crystal structure of Li_2ZrCl_6, effectively improving its stability upon exposure to humid air while simultaneously increasing its ionic conductivity. Furthermore, Jia *et al.* [79] systematically studied the doping effects of 13 different rare-earth metal elements on halide SSEs, comparing the influence of various dopants on the properties of Li_2ZrCl_6. This research provides a valuable reference for exploring suitable doping elements compatible with halide SSEs.

In summary, elemental doping optimizes the performance of SSEs by modifying their crystal structure, electronic density of states, and defect chemistry, thereby achieving multi-dimensional regulation of the interface with the LMA. Non-reactive doping (*e.g.*, Mg^{2+}, Zn^{2+}) enhances the intrinsic structural stability of the SSEs and improves their mechanical strength, suppressing lithium dendrites penetration. Interface-reactive doping (*e.g.*, Cl^-, F^-) participates in interfacial reactions to form a SEI rich in components like LiF and LiCl, reducing interfacial impedance and suppressing side reactions. Multi-element co-doping leverages synergistic effects to simultaneously optimize ionic conductivity and interfacial stability.

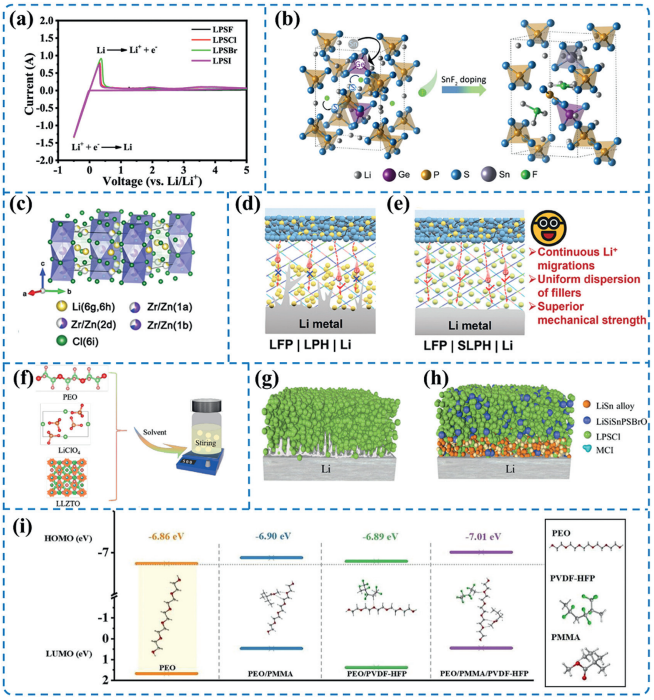


Fig. 7. (a) CV test results of the $Li_{7.3}P_{2.9}S_{10.75}X_{0.3}$ (X = F, Cl, Br, I) electrolyte systems. Reproduced with permission [75]. Copyright 2025, American Chemical Society. (b) Schematic of SnF_2-doped LGPS. Reproduced with permission [77]. Copyright 2024, Wiley-VCH. (c) Crystal structure schematic of $Li_{2.4}Zr_{0.8}Zn_{0.2}Cl_6$ prepared *via* Zn doping of Li_2ZrCl_6 (LZC). Reproduced with permission [32]. Copyright 2025, Wiley-VCH. (d) Interfacial instability induced by agglomeration of LATP particles. (e) Schematic illustrating the advantages of composite SSEs. Reproduced with permission [82]. Copyright 2025, Wiley-VCH. (f) Synthesis schematic of PEO-$LiClO_4$-LLZTO composite SSEs. Reproduced with permission [83]. Copyright 2024, Wiley-VCH. (g) Schematic of lithium dendrites at the $Li_{5.3}PS_{4.3}Cl_{1.7}$/LMA interface. (h) Schematic of stable interface between composite SSEs and LMA. Reproduced with permission [33]. Copyright 2025, Wiley-VCH. (i) Electrochemical stability windows of different composite solid polymer electrolytes. Reproduced with permission [86]. Copyright 2023, Elsevier.

3.1.4. Composite SSEs

Currently, single-component SSEs all exhibit interfacial issues when paired with the LMA. For example, inorganic SSEs, represented by oxides and sulfides, possess high ionic conductivity and mechanical strength, while they suffer from poor interfacial contact with the LMA. Although solid polymer electrolytes exhibit good flexibility, they face issues of lithium dendrites and low ionic conductivity when matched with the LMA [80]. These limitations severely hinder the development of ASSLMBs. Employing composite SSEs can improve the interfacial issues between SSEs and the LMA. The core mechanism lies in overcoming the interfacial challenges faced by single-component SSEs through the synergistic effects of multiple components, thus constructing an interface that integrates high ionic conduction, strong chemical stability, and good solid-solid contact by leveraging the complementary advantages of different SSEs [81]. Common composite strategies include organic-inorganic composite SSEs, multi-component inorganic SSEs composites, and multi-component organic SSEs composites.

In various composite SSE systems, the most common approach is the organic-inorganic composite SSE strategy. This composite strategy can effectively combine the advantages of high mechanical

strength and high ionic conductivity from inorganic SSEs with the flexibility advantage of organic SSEs. Wen *et al.* [82], to address the issues of poor interfacial performance and induced lithium dendrites in $Li_{1+x}Al_xTi_{2-x}(PO_4)_3$ (LATP) material caused by agglomeration (Fig. 7d), composited it with a polymer matrix composed of PEO and PVDF-HFP, thereby achieving superior interfacial physical contact. This composite approach constructed fast ion transport channels as shown in Fig. 7e, effectively improving poor contact and low ionic conductivity at the interface between the SSEs and the LMA. Zhang *et al.* [83] prepared a PEO-$LiClO_4$-LLZTO composite SSEs system (Fig. 7f), and demonstrated through research that 15 wt% LLZTO was uniformly dispersed without agglomeration in this system. Research using $^6Li \rightarrow {}^7Li$ isotope tracer techniques indicated that Li_2CO_3 on the LLZTO surface could act as an intermediate for lithium-ion transport between LLZTO and PEO, promoting ion transport between them and reducing lithium-ion transport resistance at the interface, thereby decreasing interfacial side reactions.

Composite strategies between different types of inorganic SSEs are also effective for improving interfacial issues. This strategy can combine the inherent advantages of different inorganic SSEs. Ge *et al.* [84] composited two sulfide SSEs, $Li_{5.5}PS_{4.5}Cl_{1.5}$ and $Li_{10}SnP_2S_{12}$. $Li_{5.5}PS_{4.5}Cl_{1.5}$ possesses excellent compatibility with the LMA, while $Li_{10}SnP_2S_{12}$ forms a Li-Sn alloy during cycling, inhibiting the formation and growth of lithium dendrites. This composite SSEs effectively suppressed the formation and growth of lithium dendrites at the interface through the synergistic effect of its components. Xu *et al.* [33], to mitigate the lithium dendrites issue at the interface between the single sulfide SSEs $Li_{5.3}PS_{4.3}Cl_{1.7}$ and the LMA, as shown in Fig. 7g, composited it with $Li_{9.54}[Si_{0.5}Sn_{0.5}]PSBrO$, which has high ionic conductivity and an interfacial passivation effect, constructing the ASSLMB system depicted in Fig. 7h.

Beyond common sulfide composites, there are also composites like $Li_{6.5}La_3Zr_{1.5}Ta_{0.5}O_{12}$ with deformable oxide glass $45Li_2SO_4$–$30Li_2CO_3$–25LiBr to enhance the interfacial stability of the SSEs with the LMA [85]. Apart from the aforementioned two composite approaches, employing composite strategies with multiple types of solid polymer electrolytes is also an effective strategy to enhance interfacial stability. Ye *et al.* [86] systematically studied the electrochemical stability windows of different types of composite solid polymer electrolytes, with results shown in Fig. 7i. Through screening and comparison with pure PEO-based SSEs, employing PMMA-PVDF-HFP composite could lower the HOMO energy level, enhance the oxidation resistance of the SSEs, and strengthen its electrochemical stability against the LMA.

As a breakthrough direction for addressing interfacial issues between SSEs and the LMA, composite SSEs will exhibit a future development trend characterized by multi-dimensional synergistic innovation alongside accelerated industrialization. In future research, the guiding principle should be optimizing the interface between SSEs and the LMA. Through precise design and cost-optimized fabrication, composite SSEs with superior comprehensive performance should be developed. Within specific research processes, machine learning screening strategies can be innovatively employed to identify compatible SSEs, accelerating the industrial deployment of ASSLMBs in scenarios demanding high energy density and high safety.

3.2. Optimization strategies for SSEs/LMA interfaces

3.2.1. Interface pressure application

Applying pressure at the SSEs/LMA interface to improve interfacial contact is an effective strategy for addressing the issue of poor solid-solid physical contact. As shown in Fig. 8a, interfacial pressure can induce creep deformation in lithium metal on the one hand, thereby filling micron-scale voids at the interface, increasing the effective contact area, and consequently reducing interfacial resistance [34]. On the other hand, interfacial pressure can physically constrain the propagation of interfacial cracks caused by volume changes, enhancing the mechanical blocking of lithium dendrites by the SSEs (especially oxide SSEs), thereby suppressing the growth of lithium dendrites at the interface. McConohy *et al.* [87] tested the effect of pressure on interfacial lithium dendrites. The research results, as shown in Fig. 8b, demonstrate that applying pressure to produce a weak strain of 0.070 % is sufficient to control and alter the propagation direction of lithium dendrites. Further studies proved that globally applied compressive stress can be used to suppress the initiation of new cracks, thereby preventing the propagation of lithium dendrites. Wang *et al.* [88] tested the effect of stacking pressure on the capacity of ASSLMB systems. The results, as shown in Fig. 8c, indicate that appropriate interfacial pressure can enhance the specific discharge capacity of the materials.

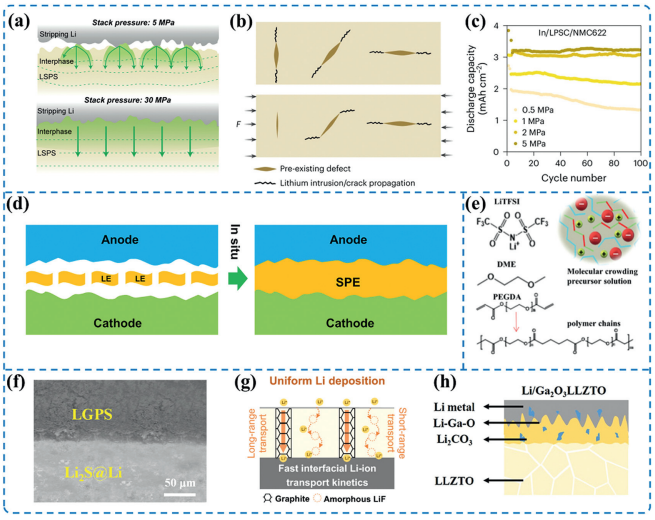


Fig. 8. (a) Schematic of interfacial pressure affecting physical contact at the LGPS/LMA interface. Reproduced with permission [34]. Copyright 2021, American Chemical Society. (b) Schematic of external pressure healing interfacial microcracks. Reproduced with permission [87]. Copyright 2023, Springer Nature. (c) Relationship between interfacial pressure and discharge specific capacity in ASSLMB systems. Reproduced with permission [88]. Copyright 2025, Springer Nature. (d) Principle schematic of *in situ* polymerization technology. Reproduced with permission [91]. Copyright 2021, Elsevier. (e) Chemical equation for polymerization reaction between PEGDA and DME. Reproduced with permission [36]. Copyright 2024, Wiley-VCH. (f) Schematic of Li_2S protective layer at LGPS/LMA interface. Reproduced with permission [97]. Copyright 2024, Wiley-VCH. (g) Schematic of high-speed ion transport channels in AFI interphase. Reproduced with permission [98]. Copyright 2025, Elsevier. (h) Schematic of Li-Ga-O layer construction at LLZTO/LMA interface. Reproduced with permission [35]. Copyright 2022, American Chemical Society.

However, pressure regulation requires balancing mechanical stability and interfacial compatibility. In practical applications, the application of pressure must be precisely controlled. Insufficient pressure fails to achieve the desired interfacial optimization effect; conversely, excessive pressure may cause brittle fracture of the electrolyte or stress concentration on the LMA surface, thereby exacerbating the risk of interfacial failure and impairing battery performance [89]. For instance, sulfide SSEs (*e.g.*, Li_6PS_5Cl) readily develop microcracks under high pressure, becoming penetration channels for lithium dendrites. In summary, applying pressure at the SSEs/LMA interface is an effective interfacial optimization strategy. By optimizing pressure parameters and application methods, it holds promise for resolving issues such as poor interfacial contact and lithium dendrites in ASSLMBs, advancing their development toward high-performance and high-safety applications.

3.2.2. In situ polymerization

In situ polymerization technology applied to ASSLMBs is a strategy that converts liquid monomer precursors into solid polymer electrolytes during battery assembly or operation. This strategy achieves molecular-level conformity and 3D interpenetration at the electrode/SSEs interface on the one hand, fundamentally resolving the solid-solid interfacial contact challenge in traditional ASSLMBs. Consequently, it further addresses interfacial limitations such as restricted lithium-ion transport and lithium dendrites growth caused by poor physical contact. On the other hand, *in situ* polymerization technology can be employed to prepare superior-performance composite SSEs. By introducing inorganic fillers (*e.g.*, LLZO, Al_2O_3 particles) into the polymerizable monomers to form a composite system, the performance of the SSEs can be further optimized [90].

The core of *in situ* polymerization technology lies in utilizing initiation methods such as thermal, photo, chemical, or electrochemical triggering to induce uniform polymerization reactions in monomers. The principle schematic is shown in Fig. 8d, with the final outcome being the construction of a high-performance interface [91]. In current research on *in situ* polymerization, the triggered monomers primarily consist of monomeric polymers. Common triggered monomers include 1,3-dioxolane (PDOL), acrylates (PNT), and polyethylene glycol diacrylate (PEGDA), among others. In studies on PDOL *in situ* polymerization, Xu *et al*. [92] innovatively employed Mg-containing montmorillonite as an initiator for DOL. Compared to conventional initiators, the PDOL prepared *via* montmorillonite initiation exhibited more uniform chain segment distribution. Moreover, an MgF_2-containing interphase formed at the interface, thereby protecting the anode interface. Similarly, when AlF_3 was used as an initiator, it also achieved anode interface protection by forming alloys and fluoride protective layers [93]. Zhou *et al*. [36] employed the crosslinking polymerization technique illustrated in Fig. 8e to perform *in situ* polymerization of PEGDA with 1,2-dimethoxyethane (DME), constructing a unique crosslinked lithium-ion channel. This ion channel endowed the solid polymer electrolyte with high ion transport efficiency. Furthermore, while maintaining excellent contact with the LMA interface, this solid polymer electrolyte possessed high mechanical strength, effectively suppressing the formation and growth of lithium dendrites at the interface.

In situ polymerization technology also plays a vital role in preparing composite SSEs. By initiating monomer polymerization *in situ* within the polymer matrix, inorganic fillers can be uniformly dispersed during polymerization, achieving tight integration between components. Gao *et al*. [94] incorporated zinc oxide nanowires (ZnO NWs) as an inorganic SSE into the PDOL *in situ* polymerization system. During lithium-ion deposition and stripping, the piezoelectric effect-generated electric field from ZnO NWs reduced local lithium-ion concentration and promoted uniform lithium-ion flux, thereby effectively inhibiting lithium dendrites growth. For composite SSEs preparation, *in situ* polymerization significantly enhances the Li^+ conductivity, mechanical properties, and interfacial stability of pure polymer SSEs.

In situ polymerization technology also possesses advantages in the manufacturing process. Its integrated design strategy effectively avoids potential contamination that traditional SSEs may encounter during processing, enhancing the overall performance and batch consistency of batteries. In future research, efforts should focus on overcoming inherent challenges of *in situ* polymerization technology, such as non-uniform polymerization, unpredictable polymerization rates, and interfacial side reactions induced by temporary residual monomers/initiators. Through rational design, the further application of *in situ* polymerization technology in resolving interface issues between LMA and SSEs should be advanced, thereby facilitating its implementation in commercial large-scale production.

3.2.3. Artificial SEI protective layer

To address the critical issue of instability at the SSEs/LMA interface, researchers have proposed designing an artificial SEI to achieve interfacial regulation [95]. The artificial SEI film forms a uniform, dense, and stable protective layer at the interface, effectively suppressing direct contact between lithium metal and the SSEs, thereby reducing interfacial side reactions. This protective layer typically exhibits excellent ion selectivity, allowing unrestricted lithium-ion transport while blocking direct electron transfer, preventing the formation and growth of lithium dendrites. Moreover, the artificial SEI can alleviate interfacial stress and enhance mechanical stability at the interface. Through rational design of the composition and structure of the artificial SEI, its performance can be further optimized to achieve effective protection of the SSEs/LMA interface. This enhances the battery's cycling stability and safety, providing crucial theoretical guidance and technical pathways for overcoming the cycle life limitations of ASSLMBs [96]. In current research, commonly reported materials for artificial SEI protective layers mainly include fluorides (LiF, SnF_2), nitrides (Li_3N, Cu_3N), oxides (Al_2O_3, ZnO, Li_2O), and sulfides (Li_2S, MoS_2), among others.

The mechanisms by which different types of artificial SEI protective layer materials function are similar: All directly form or reactively generate an interfacial protective layer that permits lithium-ion transport while blocking electrons. However, in different SSE systems, artificial SEI layers play distinct primary roles. For example, in highly reactive systems represented by sulfide SSEs, the primary function of artificial SEI is to prevent side reactions between lithium metal and the electrolyte, thereby enhancing interfacial electrochemical stability and further suppressing lithium dendrites. Wu *et al*. [97] constructed a dense, uniform Li_2S protective layer *via* chemical vapor deposition at the LGPS/LMA interface (Fig. 8f). This 2.6 μm-thick Li_2S layer prevented electrochemical decomposition of LGPS by lithium, significantly improving interfacial stability. Yue *et al*. [98] created an amorphous fluorinated interphase (AFI) composed of LiF and lithiated graphite at the LPSCl/LMA interface. The AFI layer not only effectively isolated LPSCl from interfacial reactions with the LMA but also established highly efficient lithium-ion transport channels (Fig. 8g) through its intrinsic high ionic conductivity. This promoted uniform lithium deposition, consequently inhibiting dendrite formation. In more stable but poorly contacting systems represented by oxide SSEs, artificial SEI layers primarily enhance interfacial contact to suppress lithium dendrites. Liu *et al*. [35] addressed poor physical contact at the $Li_{6.4}La_3Zr_{1.4}Ta_{0.6}O_{12}$ (LLZTO)/Li interface by: (1) Removing Li_2CO_3 impurities (formed by oxidation) from LLZTO surfaces *via* drop-casting, and (2) generating a Li-Ga-O layer (Fig. 8h) through reaction between gallium oxide and molten Li metal. This Li-Ga-O layer exhibited high compatibility with both lithium metal and the SSEs, effectively resolving interfacial contact issues.

Solid polymer electrolytes generally exhibit superior interfacial contact with LMA compared to inorganic SSEs. Therefore, the primary role of constructing an artificial SEI protective layer is to reduce side reactions between the solid polymer electrolyte and the LMA. Jabbari *et al*. [99] added partial phosphazene to the PEO electrolyte, generating nanocrystals rich in multiple materials including Li_3N, LiF, Li_3P, and Li_3PO_4. This effectively suppressed side reactions between the solid polymer electrolyte and the LMA. In research on constructing artificial SEI protective layers at SSEs/LMA interfaces, artificial SEI layers increasingly consist of multiple materials. This combines different material types to create higher-performance artificial SEI protective layers. For example, Gao *et al*. [100] prepared a Li_3N-LiF protective layer that integrates high ionic conductivity with mechanical strength. Additionally, the artificial SEI can alleviate interfacial stress and enhance mechanical stability at the interface. Through rational design of the artificial SEI's com-

position and structure, its performance can be further optimized to achieve effective protection of the SSEs/LMA interface, enhancing the battery's cycling stability and safety. In addition to traditional interface optimization strategies, some novel optimization strategies have been developed to achieve the stability of the interface between solid electrolytes and lithium anodes. Inspired by the micro-porous structure of the white sea urchin skeleton, Ma *et al.* [101] combined biomimetic design with advanced structural engineering and first applied the triply periodic minimal surface (TPMS) structure based on fluoropolymers to the interface layer design of lithium batteries. This TPMS structure not only provides channels for lithium ion transport but also suppresses lithium dendrites through the mechanical support of the skeleton and can generate a LiF protective layer on the surface of the lithium anode. Through multiple synergistic effects, it can effectively reduce the local current density, polarization and internal resistance at the interface and stabilize the anode interface. Liu *et al.* [102] used self-assembled monolayer (SAMs) technology to regulate the interface of high-energy-density lithium metal batteries. Using an Al_2O_3-coated separator as the substrate, they constructed long-range ordered polar carboxyl groups on the substrate through a simple immersion method. The ordered polar carboxyl groups generate a strong dipole moment, attracting excess electrons from Al_2O_3 to the electrolyte interface, significantly accelerating the kinetics of the carbon-fluorine bond cleavage of LiTFSI in the electrolyte, thereby constructing a LiF-rich SEI at the interface to achieve the purpose of interface protection. This low-cost and simple immersion scheme has great commercial application feasibility.

The artificial SEI protective layer strategy provides a precise control means to solve the interface stability problem between the LMA and SSEs by actively designing the interface layer. Its core advantage lies in the controllable optimization of interface chemical stability, ion transport and mechanical properties through active design. Currently, common ones such as LI and Li_3N have been applied on a certain scale. However, at present, due to the limitations of preparation complexity, compatibility contradictions and insufficient long-term stability, more artificial SEI protective layer strategies encounter bottlenecks in terms of material types and low-cost processes. Future research should focus on the design of low-cost SEI materials and the development of low-cost preparation processes to promote this strategy from the laboratory to industrialization.

3.3. LMA optimization strategies

3.3.1. Lithium alloys

Lithium metal exhibits unique advantages, including high theoretical specific capacity (3860 mAh/g) and low electrode potential (−3.04 V *vs.* SHE). Its direct contact with SSEs enables the construction of compact electrode structures, increasing volumetric energy density by over 40 %, making it the optimal choice for achieving high energy density in ASSLMB systems [103]. However, the high reactivity of lithium metal inevitably induces side reactions with SSEs during electrochemical processes. Additionally, inherent characteristics of lithium result in unavoidable lithium dendrites formation and volume changes during lithium ion deposition/stripping, significantly limiting its practical application. To address interfacial challenges in lithium metal/SSEs compatibility, researchers have developed alloy-based anodes by incorporating elements with lower reactivity into LMA [104].

In current research, common elements that can form alloys with lithium for ASSLMB anodes include In, Si, Al, Sn, Mg, Ag, Zn, Sb, *etc.*, with binary alloys being the predominant type, while ternary or multicomponent alloys constitute a smaller proportion. Compared to pure LMA, alloying elements improve the interfacial stability between anode materials and SSEs through three aspects: reducing the electrochemical reactivity of anode materials, optimizing lithium ion deposition behavior, and mitigating anode volume changes. Indium is the most commonly used element for forming lithium alloy anodes. As shown in Fig. 9a, In and Li are directly stacked at the anode side, spontaneously diffusing to form Li-In alloy during electrochemical processes [37]. This simple alloying process is highly suitable for large-scale manufacturing, but the cost of indium limits the application of Li-In alloys. To optimize costs, Li *et al.* [105] employed low-cost Sn metal to form $Li_{22}Sn_5$ alloy with lithium. Serving as a stable skeleton and uniform lithium nucleation sites, $Li_{22}Sn_5$ effectively promotes uniform lithium ion stripping/deposition, thereby significantly reducing interfacial lithium dendrites and stress, demonstrating performance markedly superior to pure LMA.

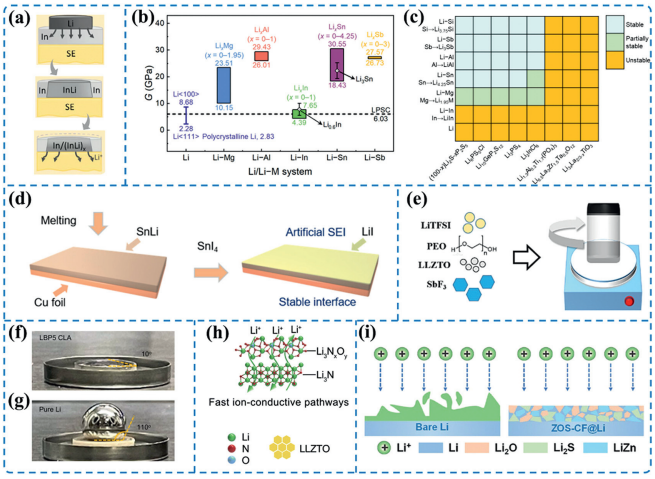


Fig. 9. (a) Schematic of self-diffusion forming Li-In alloy. Reproduced with permission [37]. Copyright 2024, Wiley-VCH. (b) Shear modulus comparison of lithium alloy types. (c) Interfacial microcrack healing under external pressure. Reproduced with permission [106]. Copyright 2024, American Chemical Society. (d) Fabrication process for LiI-protected lithium alloy anode. Reproduced with permission [107]. Copyright 2024, American Chemical Society. (e) Blending strategy for SbF_3-PEO-LLZTO composite electrolyte preparation. Reproduced with permission [108]. Copyright 2023, Elsevier. (f) Contact angle between molten Li-BP composite anode and LLZTO. (g) Contact angle of molten lithium on LLZTO surface. Reproduced with permission [111]. Copyright 2024, Elsevier. (h) Lithium ion transport channels within the composite anode bulk phase. Reproduced with permission [38]. Copyright 2023, Royal Society of Chemistry. (i) Lithiophilic host-guided uniform lithium deposition. Reproduced with permission [116]. Copyright 2024, Wiley-VCH.

To further investigate the feasibility of different alloy types in ASSLMBs, Chen *et al.* [106] systematically studied the compatibility between various lithium alloy anode materials (Li-M, M = Al, Mg, In, Sn, Sb) and different SSEs. They first evaluated the hardness of different lithium alloys through nanoindentation experiments, with shear modulus results shown in Fig. 9b Subsequently, they conducted in-depth studies on the compatibility between lithium alloys with varying hardness and different SSEs (Fig. 9c). These research findings provide theoretical guidance for selecting compatible lithium alloys and SSEs. The application of lithium alloys addresses interfacial issues in anode/electrolyte matching through three mechanisms: Enhancing interfacial mechanical properties, reducing electrochemical reactivity of LMA, and optimizing lithium ion deposition behavior at the interface. Compared with pure LMA, this approach significantly improves interfacial stability, providing crucial solutions for constructing high-stability ASSLMBs.

Beyond solely employing lithium alloys as an optimization strategy for SSEs/anode interfaces, the lithium alloy approach frequently synergizes with other optimization strategies to collectively address interfacial challenges. Common synergistic solutions include combinations with artificial protective layers. For exam-

ple, Wu *et al*. [107] immersed lithium metal in SnI_4 solution, simultaneously forming an SnLi alloy and constructing a LiI protective layer on its surface (Fig. 9d). This dual-action mechanism optimizes the interface between the SSEs and LMA. Similarly, Wang *et al*. [108] adopted a blending strategy illustrated in Fig. 9e, adding SbF_3 as an additive to the PEO-LLZTO composite SSEs system. During electrochemical processes, SbF_3 reacts *in situ* with the LMA to generate Li_3Sb and LiF, optimizing lithium deposition behavior and suppressing lithium dendrites growth at the interface. In conclusion, LMAs hold broad application prospects in ASSLMBs. While enhancing interfacial stability, they retain the intrinsic advantages of LMA, effectively improving interface stability between the anode and SSEs. Although lithium alloy anodes demonstrate significant potential for interfacial stability, challenges such as long-cycle deactivation of alloy elements and low interfacial ionic conductivity still need to be solved. This necessitates screening compatible lithium alloy anode and SSEs pairings.

The lithium alloy anode strategy enhances the interface stability between the anode and SSEs through multiple aspects such as optimizing the electrochemical potential of pure LMA, optimizing lithium-ion deposition, and improving the stability of LMA. This solution is simple in process and suitable for large-scale processing and production, with great application prospects. However, this strategy also has some limitations, such as the problem of volume change still existing and the cost increase brought about by the addition of alloying elements. In future research, focusing on exploring the types and addition ratios of inexpensive alloying elements in lithium alloys is of paramount importance for promoting the large-scale industrial application of lithium alloy anodes.

3.3.2. Composite LMA

In the LMA domain, beyond lithium alloy optimization strategies, constructing composite anodes by combining lithium metal with other material phases represents an effective solution to optimize the interface with SSEs [109]. Through the integration of lithium metal with conductive materials, porous materials, rigid framework materials, and similar components, this approach alleviates critical interfacial issues between SSEs and LMA, including lithium dendrites penetration, interfacial side reactions, and contact failure, by simultaneously improving interfacial contact, homogenizing lithium ion deposition/stripping processes, and reducing anode volume changes. These advancements provide transformative solutions for developing high-energy-density, long-cycle-life solid-state lithium metal batteries [110].

Regarding composite anode strategies, researchers have proposed various innovative solutions and interdisciplinary approaches. To address poor physical contact between LMA and SSEs, Li *et al*. [111] incorporated black phosphorus (BP) into molten lithium metal to form a composite material, which was then paired with rigid LLZTO to assemble an ASSLMB system. As shown in Fig. 9f, the composite anode demonstrates significantly better wetting behavior on LLZTO surfaces compared to the pure LMA shown in Fig. 9g This improvement arises because BP addition markedly enhances the adhesion work at the LMA/LLZTO interface, thereby strengthening physical contact. Similarly, Lu *et al*. [38] developed a composite material by combining lithium metal with superionic conductor phases Li_3N and LiN_xO_y. This composite not only significantly improves interfacial physical contact with LLZTO but also features high-speed ion transport pathways illustrated in Fig. 9h, demonstrating exceptional performance when paired with SSEs. Additionally, materials such as Si_3N_4 [112] and g-C_3N_4 [113] have shown effectiveness in enhancing interfacial contact when composited with LMA. Beyond improving physical contact, composite materials can suppress lithium dendrites formation by guiding uniform lithium deposition. Shi *et al*. [114] constructed a Li/C composite anode using conventional carbon conductive agents. This composite dynamically alters lithium stripping mechanisms with potential variations, effectively reducing "dead lithium" formation and subsequent dendrite generation. Dong *et al*. [115] integrated hydrophobic graphene flakes with hierarchical structures into LMA, successfully mitigating lithium dendrites formation during deposition. Liu *et al*. [116] designed a 3D lithiophilic host composite (Fig. 9i), where the scaffold directs lithium ions to deposit uniformly within the framework, alleviating dendrite issues caused by heterogeneous deposition. Materials including 3D copper mesh [117], $MoSe_2$ [118], and silver nanoparticles [119] have also been utilized as lithiophilic sites in composite anodes to regulate lithium deposition.

Composite anode strategies also effectively mitigate interfacial instability caused by volume fluctuations in pure LMA during electrochemical processes. A prevalent approach involves designing 3D scaffold structures to form composite anode materials with lithium. Qing *et al*. [120] fabricated a self-supporting composite LMA by embedding ultralight stainless steel mesh into a Li-B alloy. The high-strength mesh divides the Li-B alloy into grid-like compartments, significantly alleviating volume expansion during lithium deposition. Cao *et al*. [121] developed a 3D crosslinked porous $Li_2S/Li_{22}Sn_5$ framework to reduce volume changes during lithium deposition. Notably, the Li_2S component within the framework induces uniform lithium deposition and homogenizes interfacial electric fields. Beyond these materials, copper foam, nickel foam [122], CuMn bimetallic MOF [123], and 3D Ag_2Se@C [124] have also been utilized in lithium composites to suppress anode volume variations. In summary, composite LMA strategies synergistically combine mechanical confinement and chemical compatibility, providing critical engineering and commercialization pathways to address key challenges at the anode side, including lithium dendrites penetration, volume fluctuations, and poor physical contact in solid-state lithium batteries.

The composite LMA strategy improves the interface problem between the LMA and SSEs by combining lithium with other functional materials, especially in addressing the volume expansion of LMA (3D structural design), which has significant advantages and is currently a research hotspot in the field of LMA modification strategies. The key to the composite LMA strategy lies in the selection of composite material types. By using the synergistic strategy of composite materials and the LMA, the aim is to optimize interfacial contact, inhibit lithium dendrite growth, and enhance interfacial stability. However, this strategy also has both advantages and disadvantages. The preparation and composite process of composite materials increase the complexity and cost of the technology, and may face technical challenges in large-scale production.

4. Summary and outlook

The advent of SSEs effectively addresses the thermal runaway risks inherent in traditional liquid electrolytes. Furthermore, their compatibility with high-capacity LMA holds the potential to elevate the energy density of lithium-ion battery systems to 500 Wh/kg, driving comprehensive innovation in next-generation lithium-ion batteries. This positions them as the most promising electrochemical energy storage technology for the future. However, achieving scalable commercialization necessitates resolving three major challenges at the SSE/LMA interface: Poor physical contact, interfacial side reactions, and lithium dendrites formation. This review comprehensively analyzes the mechanisms, exacerbating factors, and detrimental consequences of these interface issues, from the initial SSE/Li contact stage through electrochemical cycling. Building upon this analysis, we systematically summarize current interface optimization strategies, categorized by their primary optimization targets, to advance the development of highly stable ASSLMBs. The main aspects are outlined as follows:

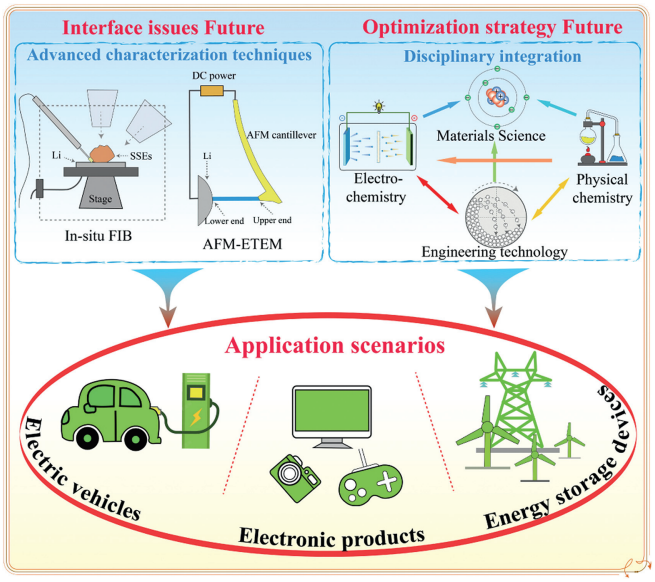


Fig. 10. Future research directions and application scenario prospects.

The interfacial issues between SSEs and LMA can be summarized as follows: (1) Poor solid-solid contact: The contact between SSEs and LMA is inherently solid-solid, leading to inadequate physical contact. This directly results in blocked ion transport and reduced energy efficiency. (2) Thermodynamic/electrochemical instability: Thermodynamic instability exists during direct contact between SSEs and LMA, while electrochemical instability occurs during battery operation. These instabilities induce interfacial side reactions, generating harmful phases that accumulate at the interface, thereby increasing interfacial resistance and depleting active materials. (3) Lithium dendrites formation: During electrochemical processes, microscale defects and inhomogeneous local electric fields cause non-uniform lithium deposition, promoting lithium dendrites nucleation and growth at the interface. This ultimately triggers short circuits and thermal runaway risks. These three major interfacial challenges severely restrict the compatibility between SSEs and LMA.

To address interfacial issues between SSEs and LMA, optimization strategies are summarized based on their primary targets: (1) On the SSEs (SSE) side: Optimizing the SSE itself, applying surface coatings, elemental doping optimizations, or compositing different types of SSEs can effectively enhance SSE stability against the LMA and mitigate lithium dendrites issues. (2) At the interface: Applying pressure or employing *in situ* polymerization technology significantly improves physical contact between the SSE and LMA; designing artificial SEI protective layers effectively isolates side reactions without impeding ion transport. (3) On the LMA side: Adopting lithium alloys or lithium-composite anode strategies reduces anode reactivity, induces uniform lithium deposition, and minimizes the damage to the interface caused by volume changes during the cycling process to the greatest extent.

In future investigations, advanced physical characterization techniques (*e.g.*, *in-situ* TEM, FIB-SEM, and ToF-SIMS) should be systematically integrated with electrochemical *in-situ* testing methods (including *in-situ* EIS, *in-situ* XRD, and *in-situ* neutron diffraction) to fundamentally elucidate the formation mechanisms of interfacial issues between SSEs and LMA. Building upon clarified interfacial mechanisms, context-specific optimization strategies should be developed through interdisciplinary integration of electrochemistry, materials science, physical chemistry, and engineering technologies (Fig. 10). This coordinated approach aims to create interface solutions with high stability, scalable manufacturability, and environmental adaptability. At the same time, it is necessary to pay attention to the application of innovative strategies such as bionic design and advanced engineering technologies (such as TPMS structure design, and SAMs technology), to promote the large-scale and commercial application of high-energy-density lithium metal all-solid-state batteries in fields such as electric vehicles, consumer electronics, and grid-scale energy storage, and to release their huge potential as the next-generation energy storage "Holy Grail".

Declaration of competing interest

The authors declare that they have no known competing financial interests or personal relationships that could have appeared to influence the work reported in this review article.

CRediT authorship contribution statement

Dongfan Li: Writing – original draft, Project administration, Funding acquisition, Conceptualization. **Jinlong Lv:** Writing – review & editing. **Jian-Cang Wang:** Writing – original draft, Methodology, Investigation, Conceptualization. **Jiaxiang Liu:** Writing – review & editing, Investigation. **Huizhe Niu:** Writing – review & editing, Investigation. **Lu Yang:** Writing – review & editing. **Hao Luo:** Writing – review & editing. **Du Lv:** Writing – review & editing. **Lichun Niu:** Writing – review & editing, Supervision, Investigation, Funding acquisition. **Zemin He:** Writing – review & editing, Supervision, Project administration, Funding acquisition. **Zongcheng Miao:** Writing – review & editing, Supervision, Project administration, Funding acquisition.

Acknowledgments

This work was supported by the National Natural Science Foundation of China (Nos. 52573348, 52173263), the National Key Research and Development Program of China (No. 2022YFB3603703), the Natural Science Basic Research Plan in Shaanxi Province of China (Nos. 2024JC-YBMS-445, S2025-JC-YB-1383), Scientific Research Fund for High Level Talents of Xijing University (No. XJ25B06), Shaanxi Changban Information Technology Co., Ltd. for their financial support (No. 2025610002002996).

References

[1] P.P. Bhawna, Shreya, et al., Ionics 31 (2025) 5263–5289.
[2] H. Sun, X. Li, B. Wu, et al., Chin. Chem. Lett. 36 (2025) 110041.
[3] E.P. Alsaç, D.L. Nelson, S.G. Yoon, et al., Chem. Rev. 125 (2025) 2009–2119.
[4] X. Li, C. Yi, W. Hu, et al., Chin. Chem. Lett. 36 (2025) 110215.
[5] G. Xiao, K. Yang, Y. Qiu, et al., Adv. Mater. 37 (2025) 2415411.
[6] X. Xiong, G. Jiang, H. Li, et al., Energy Storage Mater. 79 (2025) 104330.
[7] X. Wang, Z. He, R. Yan, et al., Chem. Eng. J. 503 (2025) 158552.
[8] Z. Ye, Z. Yu, J. Yao, et al., Chin. Chem. Lett. 36 (2025) 110272.
[9] S. Fu, P. Li, S. Yu, et al., Solid State Ionics 420 (2025) 116765.
[10] N. Wang, Y. Wei, S. Yu, et al., J. Mater. Sci. Technol. 183 (2024) 206–214.
[11] Y. Lu, Q. Wang, L. Han, et al., Adv. Funct. Mater. 34 (2024) 2314427.
[12] T. Liu, C. Paraskevoulakos, U.A. Mughal, et al., Mater. Des. 251 (2025) 113732.
[13] S. Xu, M. Han, Z. Zhu, et al., J. Materiomics 11 (2025) 100930.
[14] H. Ren, Y. Zhong, X. Lin, et al., Nano Energy 140 (2025) 111044.
[15] G. Yang, Z. Hao, C. Fang, et al., Chin. Chem. Lett. 36 (2025) 111185.
[16] Y. Luo, Z. Rao, X. Yang, et al., Energy Environ. Sci. 17 (2024) 7543–7565.
[17] S.H. Tian, J.C. Wang, N. Zhang, et al., Coord. Chem. Rev. 513 (2024) 215909.
[18] H. Niu, N. Zhang, Y. Lu, et al., J. Energy Storage 88 (2024) 111666.
[19] H. Xie, J. Feng, H. Zhao, Energy Storage Mater. 61 (2023) 102918.
[20] H.T. Sim, M.K. Oh, H.J. Kim, et al., ACS Energy Lett. 10 (2025) 2277–2284.
[21] S. Su, J. Ma, L. Zhao, et al., Carbon Energy 3 (2021) 866–894.
[22] K. Nie, Y. Hong, J. Qiu, et al., Front. Chem. 6 (2018) 616.
[23] T. Brahmbhatt, G. Yang, E.C. Self, et al., Front. Energy Res. 8 (2020) 570754.
[24] Z. Zhang, W.Q. Han, Nano Micro Lett. 16 (2024) 24.
[25] A. Machin, C. Morant, F. Marquez, Batteries-Basel 10 (2024) 29.
[26] C.Z. Zhao, B.C. Zhao, C. Yan, et al., Energy Storage Mater. 24 (2020) 75–84.
[27] C.Z. Zhao, H. Duan, J.Q. Huang, et al., Sci. China Chem. 62 (2019) 1286–1299.
[28] S.A. Pervez, M.A. Cambaz, V. Thangadurai, et al., ACS Appl. Mater. Interfaces 11 (2019) 22029–22050.

[29] Y. Lu, C.Z. Zhao, J.K. Hu, et al., Sci. Adv. 8 (2022) 0510.
[30] D. Lin, Y. Liu, Y. Cui, Nat. Nanotechnol. 12 (2017) 194–206.
[31] S. Wang, X. Xu, C. Cui, et al., Adv. Funct. Mater. 32 (2022) 2108805.
[32] P. Lei, G. Wu, H. Liu, et al., Adv. Energy Mater. 15 (2025) 2405760.
[33] F. Xu, Y. Wu, L. Wang, et al., Adv. Energy Mater. 15 (2025) 2405369.
[34] C. Lee, S.Y. Han, J.A. Lewis, et al., ACS Energy Lett. 6 (2021) 3261–3269.
[35] J. Liu, W. Guo, H. Guo, et al., Energy Fuels 36 (2022) 8500–8505.
[36] M. Zhou, W. Chen, H. Yang, et al., Adv. Energy Mater. 15 (2025) 2403082.
[37] C.D. Alt, S. Keuntje, I.L. Schneider, et al., Adv. Energy Mater. 15 (2025) 2404055.
[38] G. Lu, M. Li, P. Chen, et al., Energy Environ. Sci. 16 (2023) 1049–1061.
[39] W. Lyu, H. Fu, A.M. Rao, et al., Sci. Adv. 10 (2024) 9602.
[40] Y. Peng, X. Xiong, W. Fan, et al., Mater. Chem. Front. 8 (2024) 1421–1450.
[41] Y. Pilyugina, E.V. Kuzmina, V.S. Kolosnitsyn, ECS J. Solid State Sci. Technol. 13 (2024) 065011.
[42] P. He, Y. Tang, Z. Tan, et al., Nano Energy 124 (2024) 109502.
[43] T. Hwang, I. Chung, S. Im, et al., J. Mater. Chem. A 11 (2023) 18790–18800.
[44] M. Liu, A. Song, X. Zhang, et al., Nano Energy 136 (2025) 110749.
[45] Y. He, H. Xu, J. Shi, et al., Energy Storage Mater. 23 (2019) 418–426.
[46] C. Chang, M. Zhang, Z. Lao, et al., Adv. Mater. 36 (2024) 2313525.
[47] J.A. Lewis, F.J.Q. Cortes, Y. Liu, et al., Nat. Mater. 20 (2021) 503–510.
[48] Z. Guo, X. Li, Z. Wang, et al., J. Energy Chem. 79 (2023) 56–63.
[49] S. Wenzel, T. Leichtweiss, D. Krueger, et al., Solid State Ionics 278 (2015) 98–105.
[50] J.C. Wang, L.L. Zhao, N. Zhang, et al., Nano Energy 123 (2024) 109361.
[51] J.C. Wang, P.F. Wang, T.F. Yi, Energy Storage Mater. 62 (2023) 102958.
[52] J. Wang, L. Chen, H. Li, et al., Energy Environ. Mater. 6 (2023) e12613.
[53] S.X. Yan, Z.J. Zhao, Y. Zheng, et al., Rare Met. 44 (2025) 4446–4478.
[54] O. Sheng, J. Zheng, Z. Ju, et al., Adv. Mater. 32 (2020) 2000223.
[55] P. Peljo, H.H. Girault, Energy Environ. Sci. 11 (2018) 2306–2309.
[56] C. Bai, Y. Li, G. Xiao, et al., Chem. Rev. 125 (2025) 6541–6608.
[57] X. Wang, B. He, B. Liu, et al., Adv. Funct. Mater. 34 (2024) 2406146.
[58] X. Pei, Y. Li, T. Ou, et al., Angew. Chem. Int. Ed. 61 (2022) e202205075.
[59] Z. Gu, D. Song, S. Luo, et al., Adv. Energy Mater. 13 (2023) 2302945.
[60] J. Yao, G. Zhu, K. Dong, et al., Adv. Energy Sustain. Res. 5 (2024) 2300165.
[61] P. Luo, K. Su, Y. Wu, et al., Adv. Mater. 37 (2025) 2501142.
[62] J.C. Wang, Y. Li, Z.X. Li, et al., Energy Fuels 38 (2024) 12528–12545.
[63] H. Gao, X. Ai, H. Wang, et al., Nat. Commun. 13 (2022) 5050.
[64] A.C. Tang, E.H. Hu, B.E. Jia, et al., Rare Met. 44 (2025) 2268–2293.
[65] Z. Wang, Z. He, Z. Wang, et al., Chem. Sci. 16 (2025) 3571–3579.
[66] W. Li, J.A. Quirk, M. Li, et al., Adv. Mater. 36 (2024) 2302647.
[67] M. Xu, X. Wang, Z. Jin, et al., J. Energy Chem. 101 (2025) 685–691.
[68] Z. Jia, H. Shen, J. Kou, et al., Adv. Mater. 36 (2024) 2309019.
[69] D.K. Singh, A. Henss, B. Mogwitz, et al., Cell Rep. Phys. Sci. 3 (2022) 101043.
[70] J. Cheng, X. Zhou, H. Zhang, et al., Nano Res. 18 (2025) 94906992.
[71] H. Su, Y. Hu, M. Wang, et al., Adv. Mater. 37 (2025) 2500673.
[72] M. Liu, J.J. Hong, E. Sebti, et al., Nat. Commun. 16 (2025) 213.
[73] Z. Lu, L. Peng, Y. Rong, et al., Energy Environ. Mater. 7 (2024) e12498.
[74] C. Xu, L. Chen, F. Wu, Next Mater. 6 (2025) 100428.
[75] L. Zhou, X. Wei, J. Zhang, et al., ACS Appl. Energy Mater. 8 (2025) 473–482.
[76] X. Wu, M. Wang, H. Pan, et al., Nano Micro Lett. 17 (2025) 239.
[77] N. Zhang, Q. He, L. Zhang, et al., Adv. Mater. 36 (2024) 2408903.
[78] E. Anderson, E. Zolfaghar, A. Jonderian, et al., Adv. Energy Mater. 14 (2024) 2304025.
[79] Q. Jia, Z. Yao, J. Xiang, et al., Adv. Funct. Mater. 35 (2025) 2426053.
[80] Y. Wang, X. Zhang, X. Lang, et al., Chem. Eng. J. 508 (2025) 160824.
[81] D. Yang, X. Chen, C. Chen, et al., J. Power Sources 647 (2025) 237343.
[82] S. Wen, Z. Sun, X. Wu, et al., Adv. Funct. Mater. 35 (2025) 2422147.
[83] X. Zhang, S. Cheng, C. Fu, et al., Adv. Energy Mater. 14 (2024) 2401802.
[84] Z. Ge, N. Chen, R. Wang, et al., Chem. Eng. J. 467 (2023) 143409.
[85] H. Nagata, J. Akimoto, J. Power Sources 539 (2022) 231596.
[86] X. Ye, J. Liang, J. Hu, et al., Chem. Eng. J. 455 (2023) 140846.
[87] G. McConohy, X. Xu, T. Cui, et al., Nat. Energy 8 (2023) 241–250.
[88] C. Wang, Y. Liu, W.J. Jeong, et al., Nat. Mater. 24 (2025) 907–916.
[89] Y.T. Chen, J. Jang, J.A.S. Oh, et al., Adv. Energy Mater. 14 (2024) 2304327.
[90] L. Wan, H. Nie, Q. Yu, et al., Chem. Eng. J. 513 (2025) 162810.
[91] H. Cheng, J. Zhu, H. Jin, et al., Mater. Today Energy 20 (2021) 100623.
[92] H. Xu, J. Mi, J. Ma, et al., Energy Environ. Sci. 18 (2025) 4231–4240.
[93] X. Zhang, M. Zhang, J. Wu, et al., Nano Energy 115 (2023) 108700.
[94] H. Gao, Y. Zhou, K. Wang, et al., Adv. Energy Mater. 15 (2025) 2501379.
[95] Z. Jiang, S. Chen, C. Wei, et al., Chin. Chem. Lett. 35 (2024) 108561.
[96] K. Yu, M. Cui, Q. Wang, et al., Chem. Eng. J. 514 (2025) 163231.
[97] X. Wu, H. Pan, M. Zhang, et al., Adv. Sci. 11 (2024) e2308604.
[98] A.L. Yue, H. Yuan, S.J. Yang, et al., J. Energy Chem. 107 (2025) 277–284.
[99] V. Jabbari, V. Yurkiv, M.G. Rasul, et al., Energy Storage Mater. 57 (2023) 1–13.
[100] Q. Gao, D. Wu, Z. Wang, et al., Energy Storage Mater 63 (2023) 103007.
[101] C. Ma, S. Zou, Y. Wu, et al., Angew. Chem. Int. Ed. 63 (2024) e202402910.
[102] Y. Liu, X. Tao, Y. Wang, et al., Science 375 (2022) 739–745.
[103] T. Banerjee, R. Kundu, ACS Appl. Energy Mater. 8 (2025) 7780–7804.
[104] W.J. Jeong, C. Wang, S.G. Yoon, et al., ACS Energy Lett. 9 (2024) 2554–2563.
[105] G. Li, T. Zhang, J. Tang, et al., Adv. Mater. 37 (2025) 2417770.
[106] S. Chen, Q. Cao, B. Tang, et al., ACS Energy Lett. 9 (2024) 5373–5382.
[107] L. Wu, F. Pei, Y. Zhang, et al., ACS Energy Lett. 9 (2024) 5992–6001.
[108] A. Wang, M. Yi, S. Chang, et al., Chem. Eng. J. 474 (2023) 145593.
[109] Y. Li, Y. Xu, X. Han, et al., Chin. Chem. Lett. 35 (2024) 109189.
[110] G. Peng, Q. Fan, W. Zhang, et al., J. Alloys Compd. 1026 (2025) 180411.
[111] Z. Li, D. Tang, W. Wang, et al., Nano Energy 132 (2024) 110356.
[112] M. Yu, X. Ning, Chem. Eng. J. 503 (2025) 158554.
[113] Y. Huang, B. Chen, J. Duan, et al., Angew. Chem. Int. Ed. 59 (2020) 3699–3704.
[114] P. Shi, L.P. Hou, C.B. Jin, et al., J. Am. Chem. Soc. 144 (2022) 212–218.
[115] L. Dong, L. Nie, W. Liu, Adv. Mater. 32 (2020) 1908494.
[116] X. Liu, H. Tan, Y. Li, et al., Adv. Funct. Mater. 35 (2025) 2420382.
[117] H. Liu, Y. He, B. Jin, et al., Chem. Eng. J. 496 (2024) 154072.
[118] A. Nagendra, G. Karmakar, A. Tyagi, et al., ACS Appl. Energy Mater. 7 (2024) 7485–7495.
[119] S. Lee, Y. Lee, W.J. Song, et al., Energy Storage Mater. 73 (2024) 103850.
[120] P. Qing, Z. Wu, A. Wang, et al., Adv. Mater. 35 (2023) 2211203.
[121] L. Cao, M. Chu, Y. Li, et al., Adv. Mater. 36 (2024) 2406034.
[122] C. Guo, Y. Guo, R. Tao, et al., Nano Energy 96 (2022) 107121.
[123] T. Wei, Y. Zhou, C. Sun, et al., Nano Res. 17 (2024) 2763–2769.
[124] H.Y. Seo, Y.B. Kim, T.G. Senthamaraikannan, et al., ACS Nano 19 (2025) 6152–6164.